# Ultrahigh-pressure phases of H_{2}O ice predicted using an adaptive genetic algorithm

Min Ji, Koichiro Umemoto, Cai-Zhuang Wang, Kai-Ming Ho, and Renata M. Wentzcovitch

Phys. Rev. B **84**, 220105 — Published 13 December 2011

DOI: 10.1103/PhysRevB.84.220105

# Ultrahigh-pressure phases of $H_2O$ ice predicted using an adaptive genetic algorithm

Min Ji[1], Koichiro Umemoto[2], Cai-Zhuang Wang[1], Kai-Ming Ho[1], and Renata M. Wentzcovitch[3]
[1]*Ames Laboratory, US DOE and Department of Physics and Astronomy, Iowa State University, Ames, Iowa 50011, USA*
[2]*Department of Geology and Geophysics, University of Minnesota, Minneapolis, MN 55455, USA*
[3]*Minnesota Supercomputing Institute and Department of Chemical Engineering and Materials Science, University of Minnesota, Minneapolis, MN 55455, USA*
(Dated: November 28, 2011)

We propose three phases of $H_2O$ under ultrahigh pressure. Our structural search was performed using an adaptive genetic algorithm which allows an extensive exploration of crystal structure at density functional theory(DFT) accuracy. The sequence of pressure-induced transitions beyond ice X at 0 K should be ice X$\rightarrow$ $Pbcm \rightarrow Pbca \rightarrow Pmc2_1 \rightarrow P2_1 \rightarrow P2_1/c$ phases. Across the $Pmc2_1$-$P2_1$ transition, the coordination number of oxygen increases from 4 to 5 with a significant increase of density. All stable crystalline phases have nonmetallic band structures up to 7 TPa.

PACS numbers:

$H_2O$ ice is one of the most abundant planet forming materials and its phase diagram is of fundamental scientific interest. It is crucial for modeling the interiors of icy solar giants (Uranus and Netpune), icy satellites, and also new ocean planets being discovered right now. Up to now, sixteen crystalline phases have been identified experimentally[1–4]. Ice X is the highest-pressure phase among those identified experimentally. In this ionic phase, which exists above $\approx 70$ GPa, oxygen atoms form a bcc lattice and hydrogen atoms are located at the midpoint between two nearest-neighbor oxygen atoms. However, in Uranus and Neptune, pressure at their core-envelope boundary is estimated to be as high as 0.8 TPa[5]. Very recently, Neptune-sized icy exoplanets have been discovered[6,7]. Transitions beyond ice X can occur under these high pressure conditions and they are essential for modeling the interiors of these planets. Previously, Benoit et al.[8] and Caracas[9] predicted a phase with $Pbcm$ symmetry as the next high-pressure phase after ice X (up to 0.3 TPa). More recently, Militzer and Wilson proposed transitions from the $Pbcm$ to $Pbca$ and $Cmcm$ phases at 0.76 and 1.55 TPa, respectively[10]. Interestingly, they predicted the $Cmcm$ phase to be metallic, an important property for understanding the origin of magnetic fields in the giants. While these studies surely predict the existence of new phases, their searches using MD and phonon instability calculations explored limited regions of phase space producing structure relatively close to that of ice X. In this Letter, we report structures of solid $H_2O$ in the TPa pressure regime. They were found using a general and efficient structural search algorithm, the adaptive genetic algorithm.

The search for the lowest-enthalpy structures of ultrahigh-pressure ice is based on the Deaven-Ho genetic algorithm (GA) scheme[11]. This method combined with first-principles calculation has been proven to work very efficiently[12–15]. However, first-principles calculations are computationally very demanding for the GA scheme when there are a large number of atoms. On the other hand, GA searches using empirical model potentials are fast but suffer from inaccuracies which can lead the search to wrong structures. However, most of the child structures generated in GA are actually not favorable except in the simplest problems; many false structures have to be tried before hitting on the correct structure. Most of the computer time is spent in relaxing a large number of false candidate structures. For typical 20 atom/cell system about 600 local optimizations are required to reach global minimum[16]. Each optimization normally consists of 50-100 DFT steps with typical conjugate gradient method. For larger system, the number of local optimizations and DFT step time will increase exponentially and become undoable with current computer power. To remedy this, we introduced a structure search technique, the adaptive GA. In the scheme, we employ auxiliary model potentials to estimate the energy ordering of different competing geometries in a preliminary stage. Parameters of the auxiliary potentials are adaptively adjusted to reproduce first-principles results during the course of the GA search. This adaptive approach also allows the system to hop from one basin to another in the energy landscape leading to efficient sampling of configuration space.

In our study, we found that the packing geometry, volumes(pressures) and energy ordering of ice crystal phases at high pressures (>0.5 TPa) can be described relatively well by simple Lennard-Jones (LJ) potentials:

$$V_{LJ} = 4\varepsilon \left[ \left(\frac{\sigma}{r}\right)^{12} - \left(\frac{\sigma}{r}\right)^{6} \right]. \quad (1)$$

In the $H_2O$ system, a total of six parameters, representing the O-O, O-H and H-H interactions, are adaptively adjusted to explore structural phase space during the GA search. We initiate the search with random structures and carry out DFT calculations to get their energies, atomic forces and stress tensor. The LJ potential parameters are fitted to these structure by force-matching method[17]. Based on this auxiliary potential we perform full GA search to yield structural candidates. DFT calculations are carried out on the new GA pool and potential parameters are adaptively adjusted again. These procedures can be done iteratively until the potential parameters converge. The final LJ potential

pool population will then be examined with full DFT relaxation. Our test shows that using this adaptive scheme less than 200 sigle point DFT calculations are required to get converged auxiliary potential. The total number of candidates in the final full DFT relaxation is also limited, ususally less than 100 even for large system. The adaptive GA is approximately 100 times faster than full DFT GA for median size system(20-30 atoms) and much faster in larger systems. Thus this adaptive scheme allows a very efficient sampling of crystal structures, we can easily search relatively large systems up to 12 $H_2O$ formula units.

Details of the GA search can be found in several previous papers[12–15]. For auxiliary potential optimization we use LAMMPS code[18] and conjugate gradient method. First principles calculations are performed using density-functional theory (DFT) within PBE-type generalized-gradient approximation (GGA)[19]. Vanderbilt-type pseudopotentials[20] were generated using the following valence electron configurations: $1s^1$ and $2s^22p^4$ with cutoff radii of 0.5 and 1.4 a.u for hydrogen and oxygen, respectively. Candidate structures obtained with the adaptive GA were then refined using a harder oxygen pseudopotential with valence electron configuration of $2s^22p^43d^0$ and cutoff radius of 1.0 a.u. The cutoff energy for plane-wave expansions are 40 Ry and 120 Ry for the softer and the harder pseudopotentials respectively. Brillouin-zone integration was performed using the Monkhorst-Pack sampling scheme[21] over **k**-point meshes of spacing $2\pi \times 0.05\text{Å}^{-1}$. Structural relaxations were performed using variable-cell-shape molecular dynamics[22,23]. To test for structural stability, phonon and vibrational density of states (VDOS) calculations were carried out for candidate structures using density-functional-perturbation theory[24,25]. Zero-point motion (ZPM) effects are taken into account within the quasiharmonic approximation[26]. All first-principles calculations were performed using the Quantum-ESPRESSO[27], which has been interfaced with the GA scheme in a fully parallel manner.

Fig. 1 shows average values of the pressures and enthalpies calculated by first principles for structures in the adaptive GA pool. Target pressure of this adaptive GA search is 2 TPa. Our results show a fast convergence of the adaptive GA. After 10 iterations, LJ-potential pressures for structures in the GA pool are almost identical to first-principles DFT results. The adaptive GA search successfully predicts three structures: $Pmc2_1$ at 1 TPa, $P2_1$ at 2 TPa, and $P2_1/c$ phase at 3 TPa (Fig. 2). They consist of 4, 4, and 8 formula units, respectively. Structures with 3, 5, 6, 7, 9, 10, and 11 formula units were not energetically competitive. *Pbcm* and *Pbca* phases proposed previously were also obtained as metastable phases at these pressures. Examination of the enthalpy differences between the different competing phases (Fig. 3) shows that the sequence of pressure-induced phase transitions beyond ice X is X$\rightarrow$ *Pbcm* $\rightarrow$ *Pbca* $\rightarrow$ $Pmc2_1$ $\rightarrow$ $P2_1$ $\rightarrow$ $P2_1/c$. Static transition pressures are 0.28, 0.75, 0.89, 1.28, and 2.68 TPa, respectively. Zero-point motion strongly affects transition pressures. For X-*Pbcm*, *Pbcm*-*Pbca*, and *Pbca*-$Pmc2_1$ transitions, ZPM increases transition pressures to 0.29, 0.77, and 0.92 TPa. On the other hand, for $Pmc2_1$-$P2_1$ and $P2_1$-$P2_1/c$ transitions, ZPM greatly decreases transition pressures to 1.14 and 1.96 TPa.

The structures of these competing phases are closely related. Under compression, ice X transforms to the *Pbcm* phase and then to the *Pbca* phase by means of soft phonon related deformations[9,10]. In these three phases, all hydrogen atoms are located at the midpoint between two neighboring oxygen atoms. However, during the transition to the $Pmc2_1$ phase, two among the four hydrogen atoms bonded to the O1 oxygen jump to the octahedral interstitial sites next to two second-nearest-neighbor oxygen atoms. The arrangements of hydrogen atoms are *Pbca*-like around O1 and *Cmcm*-like around O2. Therefore, this phase is structurally intermediate between the *Pbca* and *Cmcm* phases. Its becomes metastable with respect to the *Cmcm* phase at $\sim$2.5 TPa. In ice X, *Pbcm*, *Pbca*, and $Pmc2_1$ phases, $OH_4$ tetrahedra form the basic structural unit, with connectivity varying in each phase. Across the *Pbca* to $Pmc2_1$ transition, two interpenetrating tetrahedral networks transform into a single network. Locally, hydrogen atoms around O2 try to keep two interpenetrating networks, while those around O1 atoms connect two networks into a single one. Tetrahedra around the O1 atoms are severely distorted compared to those around the O2 atoms.

The $Pmc2_1$ phase is dynamically stable up to 1.3 TPa. At $\sim$1.5 TPa, a zone-center soft mode appears. This soft mode induces a monoclinic distortion giving rise to the $P2_1$ phase. The $P2_1$ space group is a subgroup of $Pmc2_1$. In the $P2_1$ phase, the structural unit is no longer $OH_4$. The coordination number of oxygen atoms increases from 4 to 5. In X, *Pbcm*, *Pbca*, and $Pmc2_1$ phases, phonon dispersions are divided into two groups corresponding to nearly-rigid-body and internal O-H stretching motions of $OH_4$ tetrahedra, while this distinction is blurred in the $P2_1$ phase. As a result of higher coordination number, increase in H-O bond-length, and a 2.0% volume reduction across the $Pmc2_1$-$P2_1$ transition. Both $P2_1$ and $P2_1/c$ phases are dynamically stable at least up to 7 TPa, with no soft modes developing under compression.

In contrast with the metallic *Cmcm* phase predicted by[10], all three phases ($Pmc2_1$, $P2_1$, $P2_1/c$) have substantial DFT band gaps. In the $P2_1$ and $P2_1/c$ phases, the band gap decreases slowly under compression (Fig. 4), closing at $\sim$7 TPa in the $P2_1/c$ phase. Although all crystalline phases are insulating, $H_2O$ could be a good conductor at relevant conditions for two reasons: 1) protons highly mobile in the oxygen sublattice producing superionic phases at ultrahigh pressures and temperatures typical of the interiors of icy solar giants and exoplanets; 2) depending on the temperature, thermally excited carriers also contribute to increase the conductivity[28–35]. So far, only the bcc oxygen sub-lattice has been considered in the investigation of superionic phases. Our proposed crystal structures provide starting points for further investigation of conducting superionic states of these phases at ultrahigh pressures and

temperatures. They indicate that the oxygen sublattice should prefer to have hexagonal-derived structures beyond ∼0.4 TPa. This possibly implies a bcc-hcp transition in the superionic phase. Our predictions are consistent with the recent preprint by McMahon[36]. In this work the searches was carried out by ab initio random structure searching (AIRSS) method but limited to 4 $H_2O$ unit cell. Therefore the $P2_1/c$ phase with 8 $H_2O$ could not be identified. Our global searches up to 12 $H_2O$ provide more complete phase diagram of ultrahigh-pressure ice.

**Acknowledgments**

Work at Ames Laboratory was supported by the US Department of Energy, Basic Energy Sciences, Division of Materials Science and Engineering, under Contract No. DE-AC02-07CH11358, including a grant of computer time at the National Energy Research Supercomputing Centre (NERSC) in Berkeley, CA. KU and RMW's work were supported by NSF grants EAR-0757903, EAR-0810272, EAR-1047629, and ATM-0426757 (VLab). Computations at the University of Minnesota were performed at the Minnesota Supercomputing Institute and at the Laboratory for Computational Science and Engineering.

[1] V. F. Petrenko and R. W. Whitworth, *Physics of Ice*, Oxford Univ Press, Oxford (1999).
[2] C. Lobban, J. L. Finney, and W. F. Kuhs, Nature **391**, 268 (1998)
[3] C. G. Salzmann, P. G. Radaelli, A. Hallbrucker, E. Mayer, and J. L. Finney, Science **311**, 1758 (2006).
[4] C. G. Salzmann, P. G. Radaelli, E. Mayer, J. L. Finney, Phys Rev Lett **103**, 105701 (2009).
[5] T. Guillot, Phys Today **57**, 63 (2004).
[6] P. Butler, S.S. Vogt, G.W. Marcy, D.A. Fischer, J.T. Wright, G.W. Henry, G. Laughlin and J. Lissauer, Astrophys. J. **617**, 580 (2004).
[7] J. J. Lissauer et al., Nature **470**, 53 (2011).
[8] M. Benoit, M. Bernasconi, P. Focher, M. Parrinello, Phys Rev Lett **76**, 2934 (1996).
[9] R. Caracas, Phys. Rev. Lett. **101**, 085502 (2008).
[10] B. Militzer and H. F. Wilson, Phys Rev. Lett. **105**, 195701 (2010).
[11] D. M. Deaven, K. M. Ho, Phys. Rev. Lett. **75**, 288 (1995).
[12] A. R. Oganov and C. W. Glass, J. Chem. Phys. **124**, 244704 (2006).
[13] G. Trimarchi and A. Zunger, J. Phys.: Condens. Matter, **20**, 295212 (2008).
[14] M. Ji, C.-Z. Wang, and K.-M. Ho, Phys. Chem. Chem. Phys. **12**, 11617 (2010).
[15] S. Wu, K. Umemoto, M. Ji, C. Z. Wang, K. M. Ho, and R. M. Wentzcovitch, Phys. Rev. B **83**, 184102 (2011).
[16] G. Gao, A.R. Oganov,H. Wang, P. Li, Y. Ma, T. Cui and G. Zou, J. Chem. Phys. **133**, 144508 (2010).
[17] P. Brommer and F. Gähler, Phil. Mag. **86**, 753 (2006).
[18] S. Plimpton, Fast Parallel Algorithms for Short-Range Molecular Dynamics, J. Comp. Phys. **117**, 1 (1995).
[19] J. P. Perdew, K. Burke, and M. Ernzerhof, Phys. Rev. Lett. **77**, 3865 (1996); **78**, 1396.
[20] D. Vanderbilt, *Phys. Rev.* B **41**, R7892 (1990).
[21] H. J. Monkhorst and J. D. Pack, Phys. Rev. B **13**, 5188 (1976).
[22] R. M. Wentzcovitch, Phys. Rev. B **44**, 2358 (1991).
[23] R. M. Wentzcovitch, J. L. Martins, and G. D. Price, Phys. Rev. Lett. **70**, 3947 (1993).
[24] P. Giannozzi, S. de Gironcoli, P. Pavone, and S. Baroni, Phys. Rev. B **43**, 7231 (1991).
[25] S. Baroni, S. de Gironcoli, A. Dal Corso, and P. Giannozzi, Rev. Mod. Phys. **73**, 515 (2001).
[26] D. Wallace, *Thermodynamics of Crystals* (Wiley, New York) (1972).
[27] P. Giannozzi et al., J. Phys.: Condens. Matter **21**, 395502 (2009).
[28] C. Cavazzoni, G. L. Chiarotti, S. Scandolo, E. Tosatti, M. Bernasconi, and M. Parrinello, Science **283**, 44 (1999).
[29] R. Chau, A. C. Mitchell, H. W. Minich, and W. J. Nellis, J. Chem. Phys. **114**, 1361 (2001).
[30] N. Goldman, L. E. Fried, I. F. W. Kuo, and C. J. Mundy, Phys. Rev. Lett. **94**, 217801 (2005).
[31] A. F. Goncharov, N. Goldman, L. E. Fried, J. C. Crowhurst, I. F. W. Kuo, C. J. Mundy, and J. M. Zang, Phys. Rev. Lett. **94**, 125508 (2005).
[32] T. R. Mattsson and M. P. Desjarlais, Phys. Rev. Lett. **97**, 017801 (2006).
[33] E. Schwegler, M. Sharma, F. Gygi, and G. Galli, Proc. Nat. Acad. Sci. **105**, 14779 (2008).
[34] M. French, T. R. Mattsson, N. Nettelmann, and R. Redmer, Phys. Rev. B **79**, 054107 (2009).
[35] R. Redmer, T. R. Mattsson, N. Nettelmann, and M. French, Icarus **211**, 798 (2011).
[36] J. M. McMahon arXiv:1106.1941

| | | |
|---|---|---|
| $Pmc2_1$-type $H_2O$ at 1 TPa | | |
| $(a, b, c)$ | | (3.087Å, 1.890Å, 3.296Å) |
| $H_1$ | $4c$ | (0.25235, 0.39936, 0.34521) |
| $H_2$ | $2a$ | (0, 0.72441, 0.58937) |
| $H_3$ | $2b$ | (0.5, 0.02194, 0.05554) |
| $O_1$ | $2a$ | (0, 0.79553, -0.00013) |
| $O_2$ | $2b$ | (0.5, 0.71235, 0.29490) |
| $P2_1$-type $H_2O$ at 2 TPa | | |
| $(a, b, c, \beta)$ | | (1.711Å, 3.066Å, 2.825Å, 99.83°) |
| $H_1$ | $2a$ | (0.03146, -0.004190, 0.97579) |
| $H_2$ | $2a$ | (0.17734, 0.60082, 0.33256) |
| $H_3$ | $2a$ | (0.25493, 0.38266, 0.73104) |
| $H_4$ | $2a$ | (0.56268, 0.74399, 0.68952) |
| $O_1$ | $2a$ | (0.82524, 0.52141, 0.52159) |
| $O_2$ | $2a$ | (0.34462, 0.75497, 0.01421) |
| $P2_1/c$-type $H_2O$ at 3 TPa | | |
| $(a, b, c, \beta)$ | | (2.921Å, 2.890Å, 3.338Å, 117.86°) |
| $H_1$ | $4e$ | (-0.49599, 0.19043, 0.44690) |
| $H_2$ | $4e$ | (-0.14264, 0.13088, -0.07153) |
| $H_3$ | $4e$ | (-0.24986, -0.50964, -0.27537) |
| $H_4$ | $4e$ | (0.21275, 0.37363, -0.03277) |
| $O_1$ | $4e$ | (0.06825, -0.36013, -0.15960) |
| $O_2$ | $4e$ | (-0.42335, -0.37490, 0.33745) |

Table I: Structural parameters of $Pmc2_1$-, $P2_1$-, and $P2_1/c$-type $H_2O$.

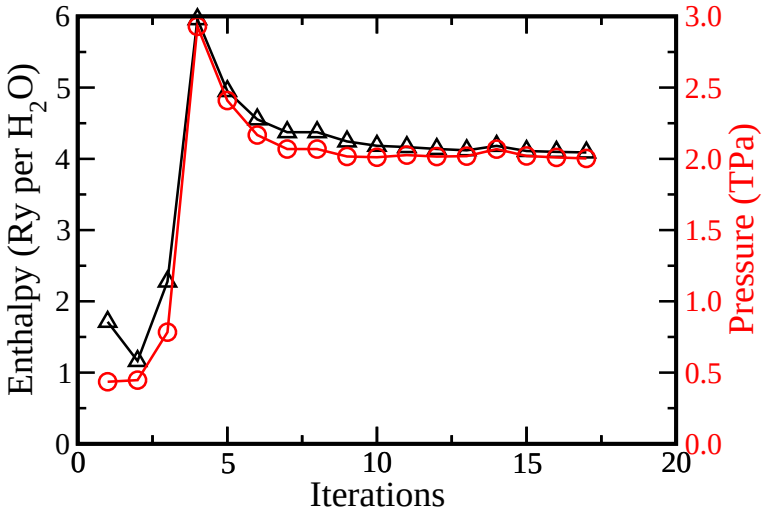


Figure 1: (Color online) Convergence of average DFT pressure(red circle) and enthalpy(black triangle) of structures in the LJ-potential GA pool as a function of adaptive potential iterations. The DFT pressure converges to the target pressure of 2 TPa after 10 iterations. The unit cell contains 8 $H_2O$ units.

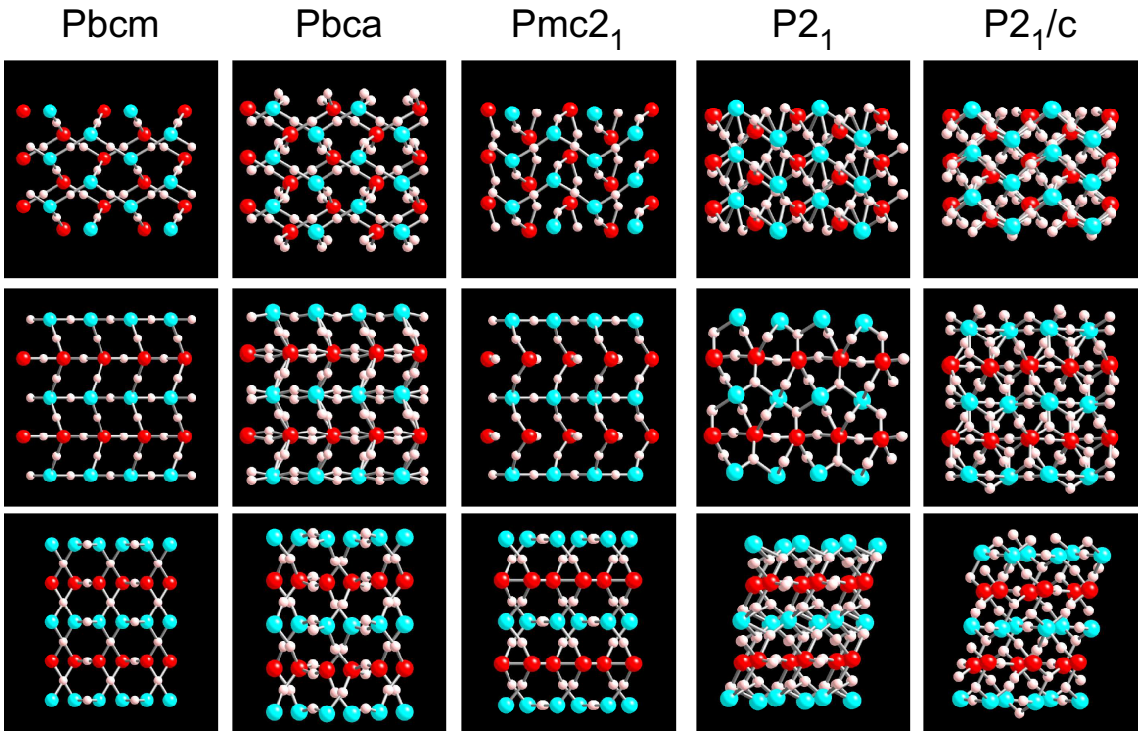


Figure 2: (Color online) Crystal structures of ultrahigh-pressure phases of ice. Blue and red large spheres denote oxygen atoms. White small spheres denote hydrogen atoms.

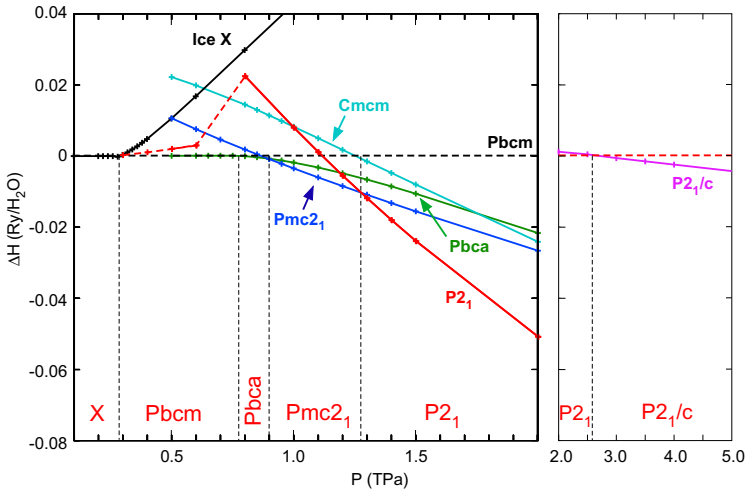


Figure 3: (Color online) Enthalpies of ultrahigh-pressure phases of ice. Dashed vertical lines denote static transition pressures.

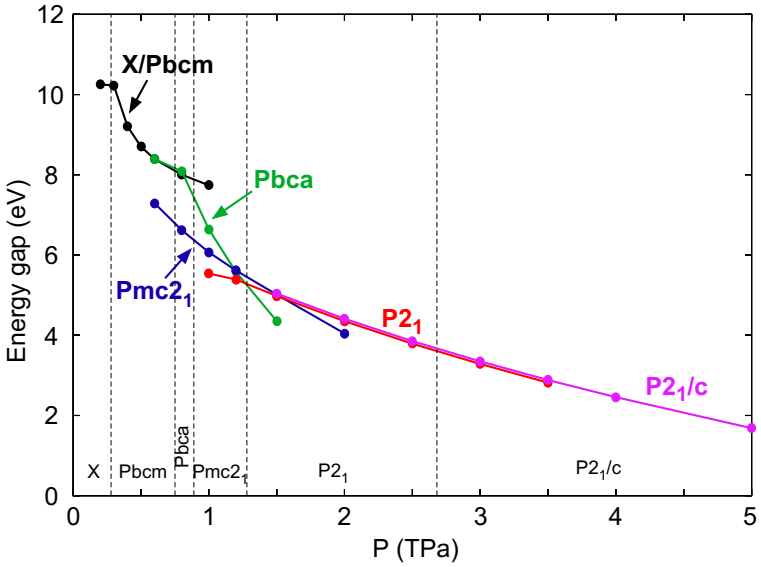


Figure 4: (Color online) Electronic band gaps of ultrahigh-pressure phases of ice. Dashed vertical lines denote static transition pressures.